Nuclear Engineering and Technology 52 (2020) 352–359

Contents lists available at ScienceDirect

Nuclear Engineering and Technology

journal homepage: www.elsevier.com/locate/net

Original Article

Effects of hydride precipitation on the mechanical property of cold worked zirconium alloys in fully recrystallized condition

Hoon Lee [a], Kyung-min Kim [a], Ju-Seong Kim [b], Yong-Soo Kim [a, *]

[a] Department of Nuclear Engineering, Hanyang University, 222 Wangsimni-ro, Seongdong-gu, Seoul, 133-791, South Korea
[b] Korea Atomic Energy Research Institute, 989-111 Daedeokdaero, Yuseong-gu, Daejeon, 305-353, South Korea

ARTICLE INFO

Article history:
Received 8 January 2019
Received in revised form
11 July 2019
Accepted 30 July 2019
Available online 30 July 2019

Keywords:
Elastic modulus
Tensile strength
Hydride precipitation
Hydride zirconium alloys
Zricaloy-4
Zirlo

ABSTRACT

The effects of hydrogen precipitation on the mechanical properties of Zircaloy–4 and Zirlo alloys were examined with uniaxial tensile tests at room temperature and at 400 °C and accompanying microstructural changes in the Zircaloy–4 and Zirlo alloy specimens were discussed. The elastic moduli of Zircaloy–4 and Zirlo alloys decreased with increasing hydrogen concentrations. Yield strengths of both materials tended to decrease gradually. The reductions of yield stress seems to be caused by the dissipation of yield point phenomena shown in stress-strain curves. Ultimate tensile strengths (UTS) of Zircaloy–4 and Zirlo slightly increased at low hydrogen contents, and then decreased when the concentrations exceeded 500 and 700 wppm, respectively. Uniform elongations were stable until 600 wppm and drops to 0% around 1400 wppm at room temperature.

1. Introduction

Understanding the mechanical property degradation of the zirconium alloys due to hydrogen is essential not only for the fuel performance evaluation during nuclear reactor operations but also for the safety assessment during dry storage conditions. During reactor operation, zirconium alloy claddings pick up hydrogen as a result of the oxidation reaction with coolant. A post-irradiation examination of spent fuels up to 55 GWD/MTU showed that the hydrogen concentration of spent nuclear cladding are up to 750 wppm [1]. It is well-known that the presence of hydrogen higher than the terminal solid solubility of hydrogen leads to hydride precipitation in the zirconium alloy matrix [2]. Hydride distributions highly depend on the microstructures and the textures of zirconium matrix [3]. Generally, cold worked stress relieved (CWSR) and recrystallized annealed (RXA) zirconium alloys have been used for fuel cladding and structural materials. The different morphologies in CWSR and RXA can affect the fracture mechanisms in CWSR and RXA [3–5].

Reactivity-Initiated Accidents (RIA) experiments [6] shows that there is a threshold burnup of brittle failures of RXA claddings which is 60 GWD/MTU. On the other hand, even though RXA is generally more ductile than CWSR, CWSR Zircaloy-4 and Zirlo claddings at 60 GWD/MTU and higher have mixed results of ductile, brittle and no failures. Radially orientated hydrides in RXA claddings simplify the failure mode into only brittle failure mode because radial hydrides can be the pathways of cracking [7]. CWSR claddings preferably have circumferential hydrides so they have a more resistance against radial crack propagation. However, when a hydride rim is formed underneath oxide layer with sufficient thicknesses, the ductility of CWSR claddings significantly drops even though the average hydrogen concentration of fuel cladding is lower than the operational design limit of 600 wppm [8].

During dry storage, the brittle failures by hydride precipitations are the major concerns of degradations [2,9]. Since safety assessments of spent nuclear fuels for dry storage has been highly demanded, the US Nuclear Regulatory Commission has integrated an assessment module for dry storage conditions into the recent version of FRAPCON-4 code [10]. Idaho National Lab has been also developing the fuel performance code, BISON, including multiphase field modeling hydride and hydride rim formation [11,12]. To predict and to formulate the effect of hydride precipitation on fuel cladding integrity, the characterization of fundamental mechanical properties such as elastic and plastic behaviors with related hydride morphologies must be preceded. In this work, cold worked

* Corresponding author.
E-mail address: yongskim@hanyang.ac.kr (Y.-S. Kim).

https://doi.org/10.1016/j.net.2019.07.032

Zircaloy-4 and Zirlo in fully recrystallized condition with uniformly distributed hydrides up to 1400 wppm, were examined using uniaxial tensile test at room temperature and 400 °C.

2. Experimental

2.1. Materials

Zirconium alloy sheets were fabricated in accordance with the ASTM specification B352. The chemical composition of the materials is presented in Table 1. To evaluate the textural information, the basal pole figure was measured by the X-ray diffraction method. Fig. 1 presents the basal pole figures of Zircaloy−4 and Zirlo. The maximum densities of basal pole are located at approximately 30° on the transverse direction. The intensity of the basal pole at ±30° of Zirlo are higher the intensity of the basal pole of Zricaloy-4. The average grain sizes observed by EBSD (Electron Back Scatter diffraction) shown in Fig. 2 was 7.15 μm at Zricaloy-4 and 3.20 μm at Zirlo. Zirlo contains the niobium element that increases mechanical strengths and recrystallization temperatures [13,14]. Therefore, Zirlo specimens have the higher peak intensity of basal pole and the smaller grain size.

2.2. Hydrogen charging and hydride morphology

Hydrogen charging to the specimens was performed at 400 °C using a Sievert's law apparatus. Since the oxide layers on the surface of specimens obstruct the hydrogen content control, the specimens were pickled in a solution of $HF:HNO_3:H_2O = 1:24:25$ and the ultra-high purity (99.9999%) hydrogen gas were used for hydrogen charging. After the hydrogen charging, the specimens were annealed at the same temperature for 10 h to ensure that hydrides were uniformly distributed. Then the specimens were slowly cooled down to room temperature with the cooling rate of 1 °C/min.

Even though we used the etchant for the surface cleaning and the ultra-high purity hydrogen gas for charging, controlling hydrogen concentration was occasionally uncertain. Therefore, hydrogen concentration was determined with the hydrogen analyzer (LECO, RH-404).

Some representative samples were etched with a solution of $HF:HNO_3:H_2SO_4:H_2O = 1:9:10:10$ to observe hydride morphologies. Fig. 3 shows the typical morphologies of hydrides observed in the Zircaloy−4 and Zirlo specimens. The morphology of hydride platelets shows that hydride platelets are parallel to the transverse direction (TD) and rolling direction (RD) in Zircaloy-4 and Zirlo.

Fig. 4 shows the hydride morphologies with hydrogen contents. The hydride platelets in Zirlo are thinker and more discrete distributions than those in Zircaloy-4. The noticeable difference in hydride morphology between Zircaloy-4 and Zirlo can be elucidated with the basal pole figures in Fig. 1. When hydrogens are charged into hcp zirconium lattice and precipitated as hydride, the hcp structure of zirconium is transformed to the fcc structure of zirconium hydride. To minimize the stacking-fault energy during the transformation from hcp to fcc, the nucleation of hydride has the relationship of {0001}hcp//{111}fcc [15]. Therefore, the hydride platelets in Zirlo are more strongly parallel to TD and RD than those in Zircaloy-4.

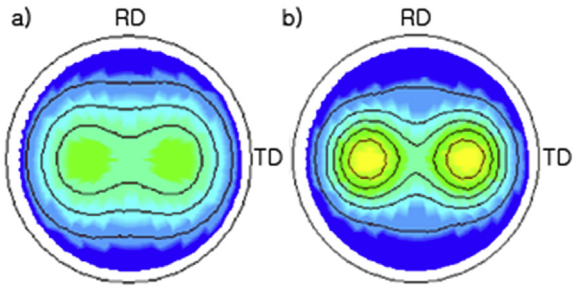

Fig. 1. Basal pole distribution of the as-received (a) Zircaloy−4 and (b) Zirlo.

2.3. Tensile test

Fig. 5 shows the detail dimensions of the tensile specimen. The sheet materials (thickness: 0.5 mm) were fabricated by EDM (electrical discharge machining) for the specimens to have the gauge section of 25.4 × 3.7 × 0.5 mm. The loading direction of specimen is parallel to TD which is corresponding to the hoop stress direction in zirconium alloy cladding.

Tensile test was conducted with the universal testing machine (Instron model 5582) at room temperature and 400 °C. The NRC recommended that the cladding temperature during dry storage must keep down below 400 °C to prevent a rupture [16]. To examine mechanical behaviors of cladding under transverse loading, 400 °C was set as the testing temperature. The strain rate was 1×10^{-3}/sec for both temperatures as recommended in ASTM E8/E21. Young's modulus was measured by the strain gauge (model KFG-6-120-C1-11) and was determined within linear sections of tensile curves according to ASTM E111. Yield stress was determined based on the 0.2% offset rule. Due to the high sensitivity of electrical type strain gauges at high temperature, elastic modulus at 400 °C was not measured.

The temperature was controlled by infrared furnace. Inert argon gas was filled in the furnace to protect the oxidation of the specimen at 400 °C. K-type thermocouples measured the temperature at three points: center, upper, and lower end of the gauge section. Temperature variation in the gauge section was less than ±2 °C. After the test, hydride morphologies and fractographies were observed by OM (Optical Microscope) and SEM (Scanning Electron Microscopy).

3. Result and discussion

3.1. Stress−strain curve of Zircaloy−4 and Zirlo sheet

Fig. 6 shows the stress-strain curves of zirconium alloys. Zirlo specimens have higher mechanical strength than Zircaloy-4 specimens as shown in yield strengths and ultimate tensile strengths in Fig. 9. As shown in Fig. 2, the smaller grain size causes the yield strength increase which in known as Hall-Petch relation. Elongations of both Zircaloy-4 and Zirlo are quite similar as shown in

Table 1
Chemical composition of zirconium alloys (wt %) and tolerance limits (±, <).

	Sn	Fe	O	Cr	C	Si	Nb	Zr
Zircaloy-4	1.3 (±0.1)	0.21 (±0.02)	0.125 (±0.02)	0.1 (±0.02)	0.012 (±0.003)	0.01 (±0.003)	-(<0.01)	Balance
Zirlo	0.95 (±0.1)	0.11 (±0.02)	0.120 (±0.02)	- (<0.01)	- (<0.01)	- (<0.008)	1.0 (±0.2)	Balance

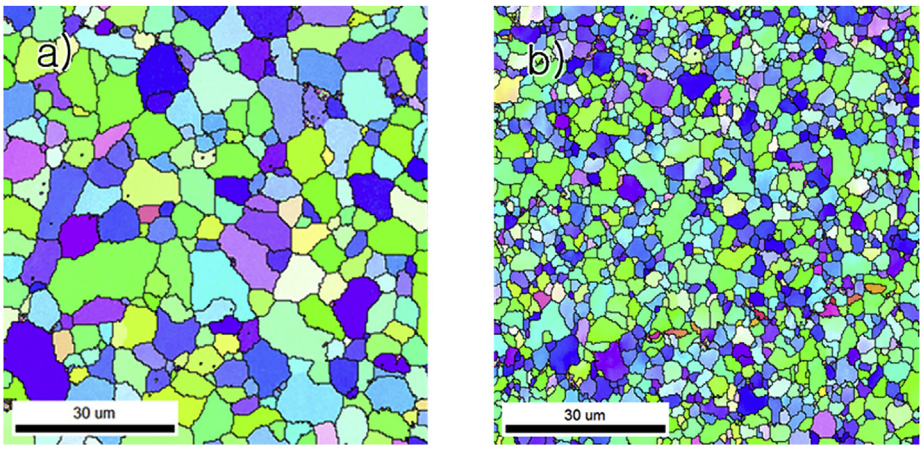

Fig. 2. EBSD map of the as-received (a) Zircaloy–4 and (b) Zirlo.

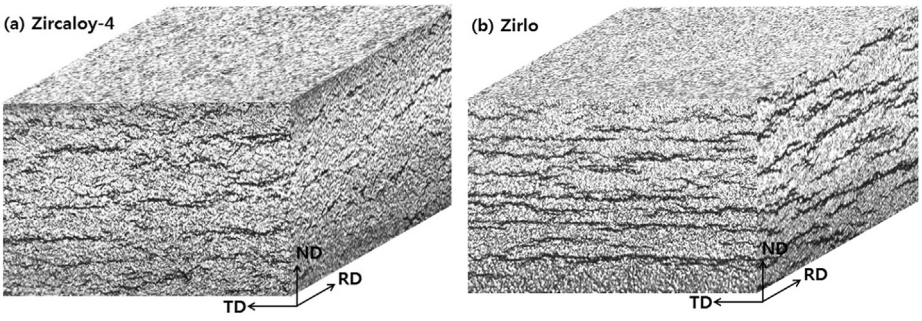

Fig. 3. Hydride morphologies of (a) Zircaloy–4 and (b) Zirlo.

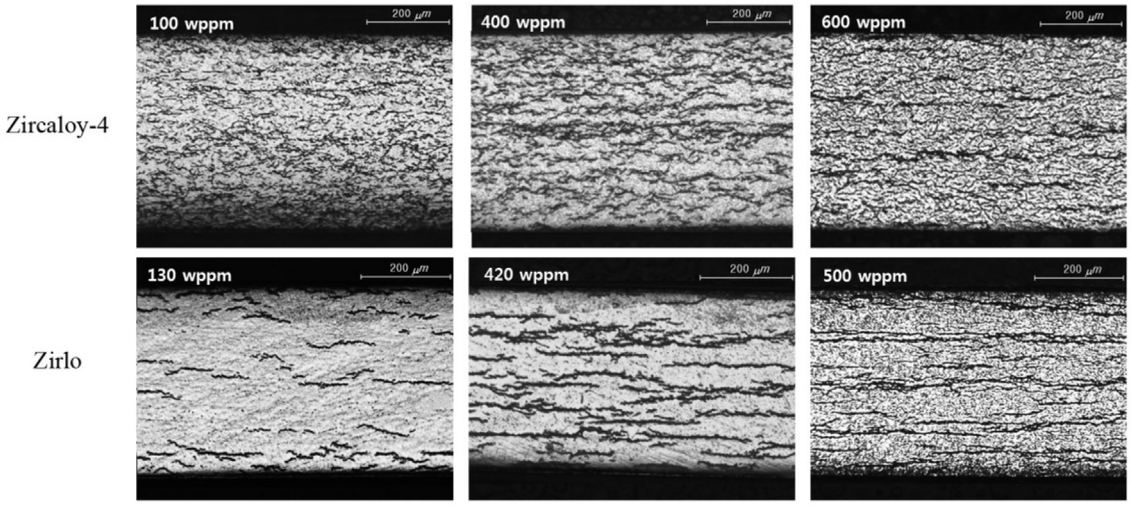

Fig. 4. Hydride morphologies of Zircaloy–4 and Zirlo with various hydrogen concentrations.

Fig. 10. At room temperature, some of specimens with higher hydrogen contents above 700 wppm were fractured without necking. Specimens with more higher hydrogen contents above 1200 wppm were fractured around yielding. If hydrogen contents were more than 1400 wppm, specimens were broken during hydrogen charging. At 400 °C, tensile stresses decrease down to the half of the values at room temperature and elongations increase by 20–30% of the values at room temperature. Fig. 7 shows true stress-true strain curves around yield points and uniform strain regions. Zircaloy-4 specimen without hydrogen has a smooth yield phenomenon whereas Zirlo specimen without hydrogen has a sharp yield phenomenon which shows higher and lower yield points and Luders band strain. The yield point phenomena gradually disappeared with increasing hydrogen contents, and the elastic-plastic transitions became more smoother.

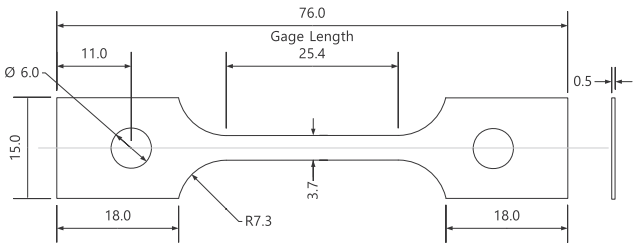

Fig. 5. Dimensions of tensile specimen.

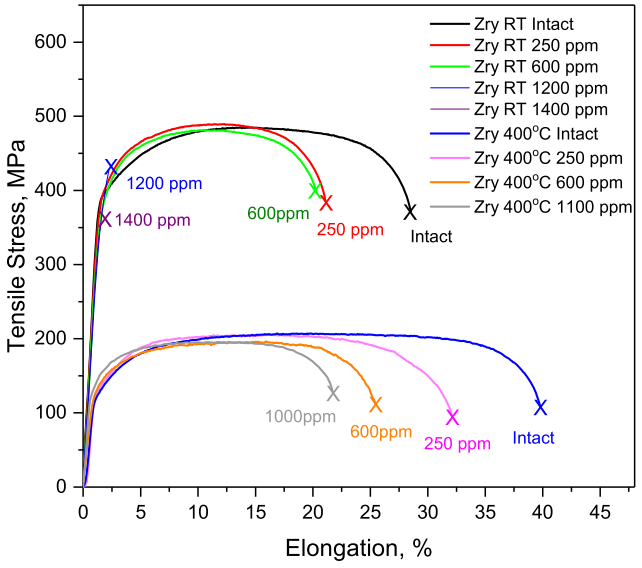

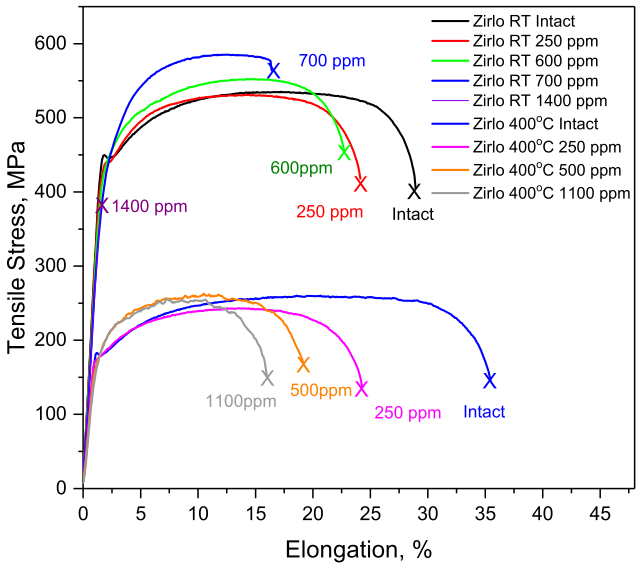

Fig. 6. Stress–strain curves of zirconium alloys (a) Zircaloy–4 and (b) Zirlo.

3.2. Elastic modulus

Fig. 8 shows the changes of elastic moduli of Zircaloy-4 and Zirlo with hydrogen concentration at room temperature. As shown in the figure, the elastic moduli of the both zirconium alloys linearly decreased with increasing hydrogen concentration. Based on the experiment data, we derived the following relationship of the elastic modulus with the hydrogen concentration for the two zirconium alloys:

$$E = 94.65 - 7.71*10^{-3} \times H \text{ for Zircaloy} - 4,$$

$$E = 93.43 - 8.46*10^{-3} \text{ x } H \text{ for Zirlo},$$

where E is the elastic modulus in GPa and H is the hydrogen concentration in weight ppm.

The similar tendency of decreasing elastic modulus with hydrogen solution and precipitated hydride can be found in some studies with dynamic elastic modulus (DEM) and macro-hardness tests. Pan et al. [17] reported that the elastic modulus of Zr alloy slightly decreased when dissolved hydrogen contents approaching terminal solid solubility (TSS). Similarly, Yamanaka et al. [18] reported that the modulus does not change or slightly increases when hydride precipitations are present in Zr alloy matrix, whereas it decreases when dissolved hydrogens are below TSS. Nano indentation experiments [19,20] show that the Young's modulus dropped rapidly at the precipitated δ–hydride phase ($ZrH_{1.6}$) due to the embrittlement of the hydride and the existence of micro-cracks in hydrides. Zirconium hydride is an incoherent second phase that can be fractured and can create micro-cracks in hydride or between hydride and matrix [15]. An experiment with acoustic emission technique [21] found that the micro-cracks in hydride initiated below the yield strength of Zr alloy and the stresses for crack initiation depend on the length of the hydrides. In addition, the micro-cracks initiated during elastic region eventually led to the decrease of ultimate tensile stress. Micro-cracks on hydride developed during elastic deformation can cause the reduction of macroscopic elastic modulus [22].

3.3. Yield strength and ultimate tensile strength

Fig. 9 shows the experimental results of YS and UTS of Zircaloy–4 and Zirlo conducted at room temperature and at 400 °C. The yield strengths of both alloys decrease gradually at room temperature with different rates as a function of hydrogen concentrations. Specifically, 18% decrease (442 MPa at 0 wppm to 361 MPa at 1400 wppm) was observed in Zirlo specimens, while approximately 10% (393–347 MPa) was observed in Zircaloy–4. As shown in Fig. 7, the yield-point phenomena gradually disappeared with increasing hydrogen concentration and 0.2%-offset yield stress decreased as well.

The yield-point phenomena are commonly caused by alloy elements, grasping dislocation movements. The diminishment of the yield-point phenomena with increasing hydrogen contents can be explained by the two mechanisms, Orowan hardening and hydrogen-induced plasticity. When hydride precipitation becomes an incoherent phase, Orowan hardening mechanism becomes dominant and inversely the shielding mechanism of dislocations becomes weaker [15]. Another mechanism is hydrogen-induced plasticity that dissolved hydrogen reduces staking fault energy and consequently increases the mobility of dislocations [23]. Due to Orowan hardening and hydrogen-induced plasticity, the hydrogen charged zirconium alloys have lower flow stresses but higher hardening rates. As shown Fig. 7, it seems that Orowan hardening mainly occurred on Zirlo specimen and eventually increase UTS (ultimate tensile strength). On the other hand, Zircaloy-4 specimens have also higher work hardenings in the early stage of plastic deformation. However, UTS does not change significantly. Rupa et al. [24] also reported the same observation of the diminishment

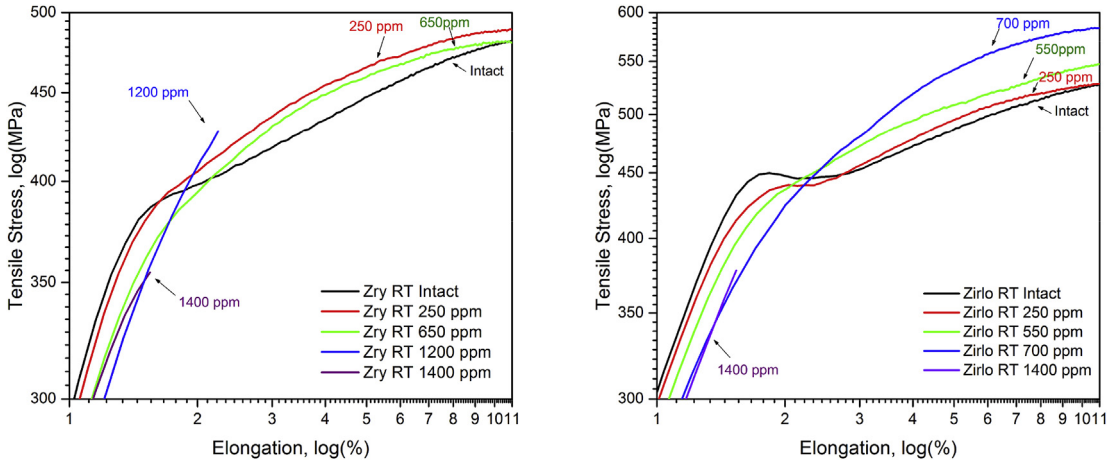

Fig. 7. Ture stress-true strain curves around yield points and uniform strain regions.

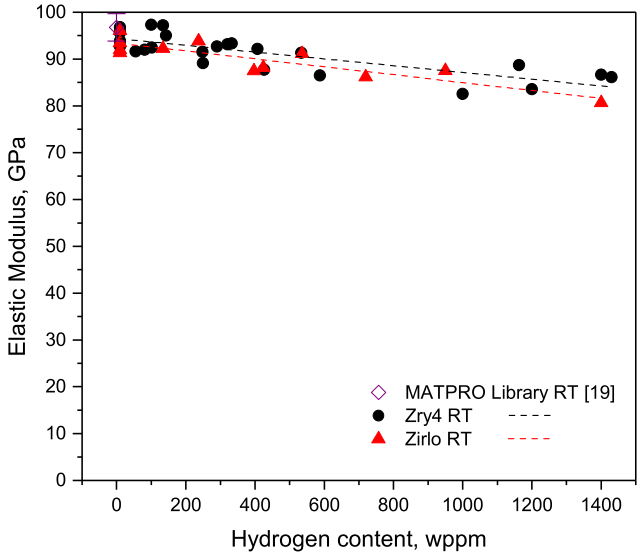

Fig. 8. Hydrogen effect on Young's modulus of Zircaloy–4 and Zirlo at room temperature and MATPRO.

of the yield-point phenomena and the increment of hardening rate. Rupa et al. commented on that the weak hardening is the combined effect of internal phase stress of hydride and hydrogen-induced plasticity by dissolved hydrogen.

As shown in Fig. 8, UTS of both Zircaloy-4 and Zirlo similarly increase until 600 wppm. However, when the hydrogen concentration exceeded 600 wppm, UTS of Zirlo specimens kept increasing until 950 wppm but UTS of Zircaloy-4 decreased. This observation of different work hardening behaviors can be explained with the effect of the preferred basal orientations. Zirlo specimens have stronger basal orientations so that the hydrides in Zirlo are more parallel to the loading direction (transverse direction) than the hydrides in Zircaloy-4. Therefore, the hardening by hydride in Zricaloy-4 is weaker because more radially orientated hydrides are formed in Zricaloy-4.

Generally, residual stresses on hydride precipitations and dislocations generated from the hydride formation act as strengthen sources in the alloy. However, there have been contradictory reports on mechanical properties of zirconium hydride because of complicated mechanical interactions between hydride and matrix. Both yield strength and UTS slightly increased [25,26]. Yield strength increased but UTS decreased [27]. Yield strength did not change but UTS increased [28]. Both yield strength and UTS slightly decreased or did not change [4]. The results in the present study is in a good agreement with Lin et al. [27] that UTS are slightly increases with hydrogen content until 400 wppm but decrease at higher hydrogen content. In addition, Bai et al. [4] conducted tensile test with various heat treated Zircaloy-4 at room temperature and 350 °C. They showed that hydrogen contents did not significantly influence the tensile strength in lower hydrogen concentration, but the tensile strength tended to decrease at higher hydrogen concentration. Bai et al. commented that precipitation generally induces hardening but hydride precipitation in Zr alloys may deplete hardening because tensile residual stresses such as micro-cracks around hydride precipitation developed in matrix.

At 400 °C, the influences of hydrogen content on mechanical strengths of both Zircaloy-4 and Zirlo were minor. Zircaloy-4 at 400 °C have no yield-point phenomena and no yield stress decrease. However, in Zirlo at 0 wppm at 400 °C the yield-point phenomenon which is the higher and lower yield points still remains at the higher temperature and gradually disappears with increasing hydrogen contents. The yield-point phenomenon in Zirlo results in slight yield stress decrease with increasing hydrogen contents. However, because the Zircaloy-4 sample at 400 °C does not have clear yield points, the yield stress of Zirclaoy-4 sample at 400 °C does not significantly change with increasing hydrogen contents. At 400 °C, no significant hardenings by hydride were observed. UTS of Zircaloy-4 specimens at 400 °C slightly decrease with hydrogen contents. However, UTS of Zirlo specimens at 400 °C does not change. All samples at 400 °C were fractured after necking. However, at room temperature, UTS varies significantly because some samples were fractured before necking when they have higher hydrogen contents and the changes of work hardening with hydrogen contents were considerable. At the higher temperature, the rates of work hardening in the beginning of plastic deformation increased with hydrogen contents as shown in Fig. 6 but do not contribute to increasing UTS. Because samples are ductile at the higher temperature, hydride precipitations only partially disturb dislocation flows and dislocation pile-ups on the precipitations becomes insignificant.

3.4. Elongation and fractography

Fig. 10 clearly shows the reductions of elongations. At room temperature, the total elongations of both Zircaloy-4 and Zirlo decreases from 27% at 0 wppm to 20% at 600 wppm and drastically

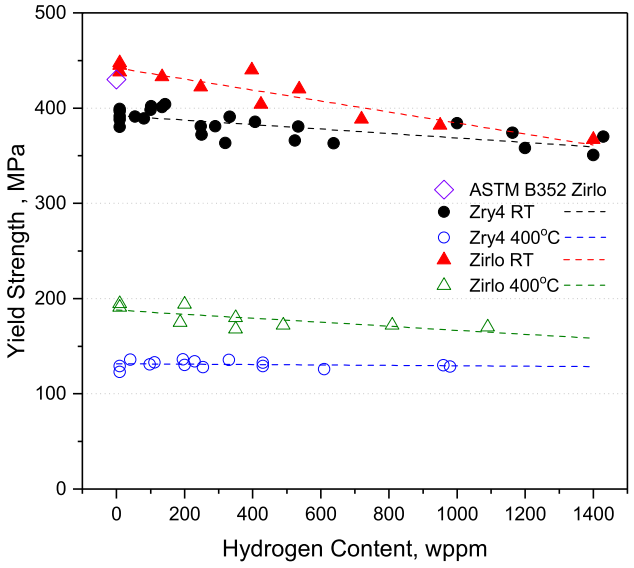

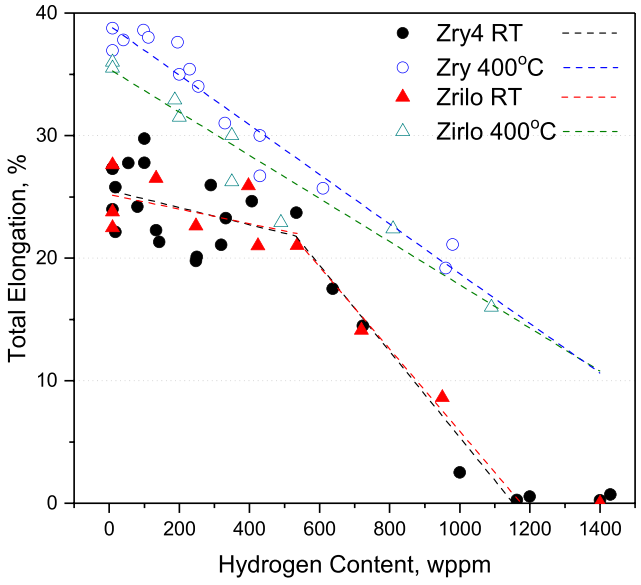

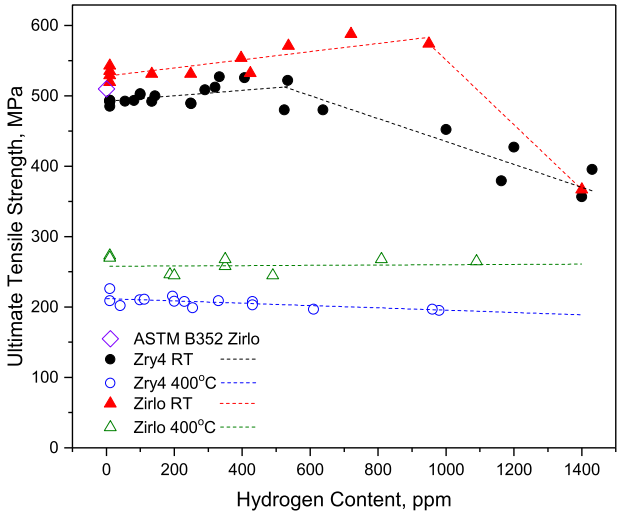

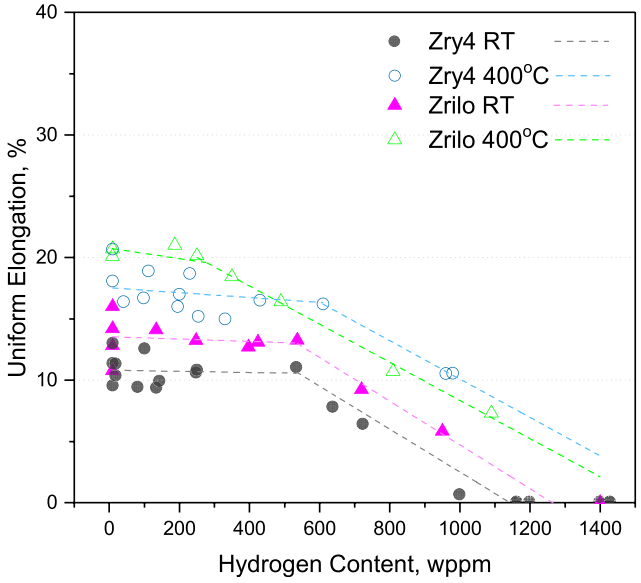

Fig. 9. Hydrogen effects on UTS and YS of Zircaloy–4 and Zirlo at room temperature and at 400 °C.

Fig. 10. Total and uniform elongations of Zircaloy–4 and Zirlo as a function of hydrogen content.

reduced to 0% around 1200 wppm. At 400 °C, the total elongations of Zircaloy-4 and Zirlo decreased from 38% of Zircaloy-4 and 35% of Zirlo at 0 wppm to around 15% around 1100 wppm. At lower hydrogen, hydride precipitations have no effect on the reduction of uniform elongation. The uniform elongations of Zircaloy-4 and Zirlo at room temperature maintained until 600 wppm. However, the uniform elongation of Zirlo specimens at 400 °C maintained only until 300 wppm and even decreased below the uniform elongation of Zircaloy-4 when hydrogen contents increase.

It has been known that the ductile rupture of zirconium alloys can be triggered by micro-cracks from hydride precipitates. Thus, many studies have been carried out on hydride fracture criteria and micro-crack growth [21,28–30]. Zirlo at 0 wppm has more uniform elongations and UTS than Zircaloy-4 because it has more strength on flow localizations. However, the uniform elongations of Zirlo specimen above 500 wppm at 400 °C are lower than those of Zircaloy-4. As shown Fig. 6 plastic instabilities before necking were noticeable in Zirlo specimen above 500 wppm at 400 °C. A possible explanation of lower uniform elongation in Zirlo can be explained as an unstable plastic deformation by the effect of abundant grain boundaries in Zirlo and incoherent hydrides [31]. However, the inconsistent behavior of the uniform strain of Zirlo may be an inconclusive result in this paper since there are limited test conditions.

Fig. 11 shows fractured surfaces of hydrided Zircaloy-4 and Zirlo. On the fracture surfaces at room temperature, we observed local cracks in the ductile matrix of the hydrided Zircaloy-4 and Zirlo with 300 and 400 wppm, respectively. At 600 and 700 wppm, quasi-cleavage, the mix of cleavage and ductile tear ridges, were found with hydrogen-induced cracks. In the both alloys with 1400 wppm, hydrogen-induced inter-granular cracks with cleavage

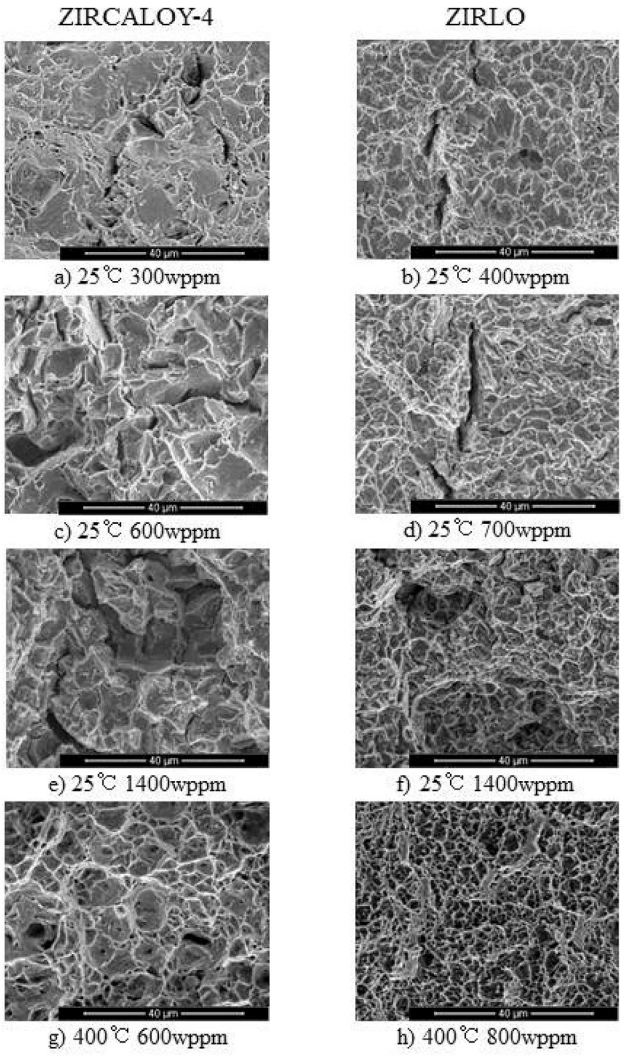

Fig. 11. Scanning electron microscopy fractography images of Zircaloy−4 and Zirlo at various conditions.

micro-facet were observed. The inter-granular size is correlated with the grain size shown in Fig. 2. Therefore, the inter-granular fractures at 1400 wppm reflects the brittle failure mode that the fractures were occurred by the segregation of densely precipitated hydrides in the grain boundary [32].

4. Conclusions

The effects of hydrogen precipitation on the mechanical properties of Zircaloy-4 and Zirlo were examined with uniaxial tensile test at the room temperature and 400 °C, to produce the mechanical property data and to support the modeling of cladding tube in normal operation and in dry storage condition.

The elastic moduli of the both zirconium alloys gradually decreased with increasing hydrogen concentration. The both zirconium alloys showed very similar results of decreasing by 10% as hydrogen concentration increased up to 1400 wppm. Based on the experiment data, the elastic modulus expression were derived as a function of hydrogen concentration for the two zirconium alloys:

$$E = 94.65 - 7.71*10^{-3}x\ H \text{ for Zircaloy} - 4,$$

$$E = 93.43 - 8.46*10^{-3}x\ H \text{ for Zirlo},$$

where E is the elastic modulus in GPa and H is the hydrogen concentration in weight ppm.

Yield strengths of both materials tended to linearly decrease at room temperature. At high temperature, Zirlo specimens showed slight decrease whereas Zircaloy-4 specimens were hardly influenced by hydrogen content. The reductions of yield stress seem to be caused by the dissipation of yield point phenomena as shown in stress-strain curves.

Ultimate tensile strengths of both hydrided Zircaloy-4 and Zirlo alloys tended to slightly increase with increasing hydrogen content and then rapidly decreased when the concentration exceeded 500 wppm in Zircaloy-4 and 700 wppm in Zirlo. However, at 400 °C, the tensile strengths were not affected by hydrogen concentration.

Uniform elongations were constantly stable until 600 wppm and drops to 0% around 1400 wppm at room temperature. At 400 °C, the uniform elongations of Zircaoy-4 were also constantly stable until 600 wppm but the elongations of Zirlo were stable only until 300 wppm and then became lower than those of Zircaloy-4. The fractography shows that both quasi-cleavage and intergranular fracture were observed at 600 and 1400 ppm, respectively.

Acknowledgements

This work was supported by the Human Resources Program in Energy Technology of the Korea Institute of Energy Technology Evaluation and Planning (KETEP), granted financial resources from the Ministry of Trade, Industry, & Energy, Republic of Korea (No. 20184030201970) and by a National Research Foundation of Korea (NRF) grant funded by the Korean government (MSIP: Ministry of Science, ICT, and Future Planning) (No. NRF-2017M2B2B1072888).

Appendix A. Supplementary data

Supplementary data to this article can be found online at https://doi.org/10.1016/j.net.2019.07.032.

References

[1] J. Kim, H. Yoon, D. Kook, Y. Kim, A study on the initial characteristics of domestic spent nuclear fuels for long term dry storage, Nucl. Eng. Technol. 45 (3) (2013) 377–384.
[2] J.S. Kim, Y.J. Kim, D.H. Kook, Y.S. Kim, A study on hydride reorientation of Zircaloy-4 cladding tube under stress, J. Nucl. Mater. 456 (2015) 246–252.
[3] T. Sugiyama, M. Umeda, T. Fuketa, H. Sasajima, Y. Udagawa, F. Nagase, Failure of high burnup fuels under reactivity-initiated accident conditions, Ann. Nucl. Energy 36 (3) (2009) 380–385.
[4] J.B. Bai, C. Prioul, D. François, Hydride embrittlement in ZIRCALOY-4 plate: Part I. Influence of microstructure on the hydride embrittlement in ZIRCALOY-4 at 20 °C and 350 °C, Metall. Mater. Trans. A 25 (6) (1994) 1185–1197.
[5] H.H. Hsu, M.F. Chiang, Y.C. Chen, The influence of hydride on fracture toughness of recrystallized Zircaloy-4 cladding, J. Nucl. Mater. 447 (1–3) (2014) 56–62.
[6] C. Vitanza, A review and interpretation of ria experiments, Nucl. Eng. Technol. 39 (5) (Oct. 2007) 591–602.
[7] J.S. Kim, T.H. Kim, D.H. Kook, Y.S. Kim, Effects of hydride morphology on the embrittlement of Zircaloy-4 cladding, J. Nucl. Mater. 456 (2015) 235–245.
[8] F. Nagase, T. Fuketa, Investigation of hydride rim effect on failure of zircaloy-4 cladding with tube burst test, J. Nucl. Sci. Technol. 42 (1) (2005) 58–65.
[9] J.S. Kim, J.D. Hong, Y.S. Yang, D.H. Kook, Rod internal pressure of spent nuclear fuel and its effects on cladding degradation during dry storage, J. Nucl. Mater. 492 (2017) 253–259.
[10] K.J. Geelhood, W. Luscher, Frapcon-4.0: A Computer Code for the Calculation of Steady-State, Thermal-Mechanical Behavior of Oxide Fuel Rods for High Burnup, U.S. Dep. Energy, 2015.
[11] D.S. Stafford, Multidimensional simulations of hydrides during fuel rod lifecycle, J. Nucl. Mater. 466 (2015) 362–372.
[12] O. Courty, A.T. Motta, J.D. Hales, Modeling and simulation of hydrogen behavior in Zircaloy-4 fuel cladding, J. Nucl. Mater. 452 (1–3) (2014) 311–320.

[13] S. Oh, C. Jang, J.H. Kim, Y.H. Jeong, Effect of Nb on hydride embrittlement of Zr-xNb alloys, Mater. Sci. Eng. A 527 (6) (2010) 1306–1313.
[14] R.P. Siqueira, H.R.Z. Sandim, T.R. Oliveira, D. Raabe, Composition and orientation effects on the final recrystallization texture of coarse-grained Nb-containing AISI 430 ferritic stainless steels, Mater. Sci. Eng. A 528 (9) (2011) 3513–3519.
[15] J.W. Martin, Precipitation Hardening, Butterworth-Heinemann, 1998.
[16] US NRC, Spent Fuel Project Office, Interim Staff Guidance-11, Revision 3, 2003.
[17] Z.L. Pan, M.P. Puls, I.G. Ritchie, Measurement of hydrogen solubility during isothermal charging in a Zr alloy using an internal friction technique, J. Alloy. Comp. 211–212 (C) (1994) 245–248.
[18] S. Yamanaka, et al., Characteristics of zirconium hydrogen solid solution, J. Alloy. Comp. 372 (1–2) (Jun. 2004) 129–135.
[19] M.P. Puls, S.Q. Shi, J. Rabier, Experimental studies of mechanical properties of solid zirconium hydrides, J. Nucl. Mater. 336 (1) (2005) 73–80.
[20] J. Xu, S.Q. Shi, Investigation of mechanical properties of ε-zirconium hydride using micro- and nano-indentation techniques, J. Nucl. Mater. 327 (2–3) (2004) 165–170.
[21] S. Shi, M.P. Puls, Fracture strength of hydride precipitates in Zr ± 2 . 5Nb alloys 275 (1999) 312–317.
[22] C.S. Fernanda, C. Alho, J.F. Labuz, Experiments on effective elastic modulus of two-dimensional solids with cracks and holes 33 (28) (1996) 4119–4130.
[23] H.K. Birnbaum, P. Sofronis, Hydrogen-enhanced localized plasticity-a mechanism for hydrogen- related fracture 176 (1994) 191–202.
[24] N. Rupa, M. Clavel, P. Bouffioux, C. Domain, A. Legris, About the mechanisms governing the hydrogen effect on visrnplastieity of unirradiated fully annealed zircaloy-4 sheet, Zircon. Nucl. Ind. Thirteen. Int. Symp. ASTM STP 1423 (2002) 811–836.
[25] H. Li, et al., Hydride precipitation and its influence on mechanical properties of notched and unnotched Zircaloy-4 plates, J. Nucl. Mater. 436 (1–3) (2013) 84–92.
[26] J.H. Huang, S.P. Huang, Effect of hydrogen contents on the mechanical properties of Zircaloy-4, J. Nucl. Mater. 208 (1–2) (1994) 166–179.
[27] S.-C. Lin, M. Hamasaki, Y.-D. Chuang, The effect of dispersion and spheroidization treatment of δ zirconium hydrides on the mechanical properties of zircaloy, Nucl. Sci. Eng. 71 (3) (1979) 251–266.
[28] M. Grange, J. Besson, E. Andrieu, Anisotropic behavior and rupture of hydrided ZIRCALOY-4 sheets, Metall. Mater. Trans. A Phys. Metall. Mater. Sci. 31 (3) (2000) 679–690.
[29] B.V. Cockeram, K.S. Chan, In situ studies and modeling the fracture of Zircaloy-4, J. Nucl. Mater. 393 (3) (2009) 387–408.
[30] M. Le Saux, J. Besson, S. Carassou, C. Poussard, X. Averty, Behavior and failure of uniformly hydrided Zircaloy-4 fuel claddings between 25 °C and 480 °C under various stress states, including RIA loading conditions, Eng. Fail. Anal. 17 (3) (2010) 683–700.
[31] Z.X. Wu, Y.W. Zhang, M.H. Jhon, D.J. Srolovitz, Anatomy of nanomaterial deformation: grain boundary sliding, plasticity and cavitation in nano-crystalline Ni, Acta Mater. 61 (15) (2013) 5807–5820.
[32] S.M. Myers, et al., Hydrogen interactions with defects in crystalline solids, Rev. Mod. Phys. 64 (2) (1992) 559–617.